

Mopra line survey mapping of NGC 6334 I and I(N) at 3 mm

A. J. Walsh^{1,2*}, S. Thorwirth^{3,4}, H. Beuther⁵ and M. G. Burton¹

¹*School of Physics, University of New South Wales, Sydney, 2052 NSW, Australia*

²*Centre for Astronomy, School of Engineering and Physical Sciences, James Cook University, Townsville, QLD 4811, Australia*

³*I. Physikalisches Institut, Universität zu Köln, Zùlpicher Str. 77, 50937 Köln, Germany*

⁴*Max-Planck-Institut für Radioastronomie, Auf dem Hügel 69, 53121 Bonn, Germany*

⁵*Max-Planck-Institut für Astronomie, Königstuhl 17, 69117 Heidelberg, Germany*

21 November 2018

ABSTRACT

A $5' \times 5'$ region encompassing NGC 6334 I and I(N) has been mapped at a wavelength of 3 mm (from 83.5 to 115.5 GHz) with the Mopra telescope at an angular resolution between $33''$ and $36''$. This investigation has made use of the recently installed 3 mm MMIC receiver and the Mopra Spectrometer (MOPS) with broadband capabilities permitting total coverage of the entire frequency range with just five different observations. In total, the spatial distribution of nineteen different molecules, ions and radicals, along with additional selected isotopologues have been studied. Whilst most species trace the sites of star formation, CH_3CN appears to be most closely associated with NGC 6334 I and I(N). Both CN and C_2H appear to be widespread, tracing gas that is not associated with active star formation. Both N_2H^+ and HC_3N closely resemble dust continuum emission, showing they are reliable tracers of dense material, as well as the youngest stages of high mass star formation. Hot ($E_u/k > 100\text{ K}$) thermal CH_3OH emission is preferentially found towards NGC 6334 I, contrasting with I(N), where only cold ($E_u/k < 22\text{ K}$) thermal CH_3OH emission is found.

Key words: circumstellar matter – infrared: stars.

1 INTRODUCTION

NGC 6334 is a giant molecular cloud located at a distance of 1.7 kpc (Neckel 1978) in the southern Galactic plane. Lying along a gas filament of 11 pc in length, NGC 6334 exhibits several luminous sites of massive star formation – as seen in the far-infrared (McBreen et al. 1979, five sources denoted using roman numerals I to V) and radio continuum (Rodriguez et al. 1982, six sources denoted with letters from A to F) with source I dominating the millimetre to the far infrared (Sandell 2000). In close proximity to NGC 6334 I, about two arcminutes to the north, another bright source is found in the millimetre- and submillimetre continuum, denoted NGC 6334 I(N) (Cheung et al. 1978; Gezari 1982; Sandell 2000). While this source is believed to be a comparably young object – as concluded from the lack of H II regions and mid-IR emission – there is compelling evidence however, that star formation is going on there (e.g. Megeath & Tieftrunk 1999). It is this twin core system, NGC 6334 I and I(N), that offers the rare opportu-

nity to study the evolution of high mass stars from the same parental cloud and in a relatively small spatial region.

Single dish molecular line observations show both cores to be chemically rich (Thorwirth et al. 2003) with source I being comparable in line density to prototypical hot cores such as Orion-KL and SgrB2(N) (Bachiller & Cernicharo 1990; McCutcheon et al. 2000; Thorwirth et al. 2003; Schilke et al. 2006). High spatial resolution observations towards both cores have been conducted: ATCA investigations of NH_3 emission up to the (6,6) inversion transition reveals the presence of warm gas in both cores (Beuther et al. 2005, 2007) and SMA continuum observations at 1.3 mm (Hunter et al. 2006) resolve each core into a sample of subcores of several tens of solar masses each, four for source I and seven for I(N), demonstrating the formation of star clusters.

Several line mapping studies using standard molecular tracers were carried out in the past to obtain information about the large scale spatial distribution of molecular gas (Kraemer & Jackson 1999; McCutcheon et al. 2000) additionally leading to the detection of several molecular outflows associated with both cores (Bachiller & Cernicharo 1990; Megeath & Tieftrunk 1999; Leurini et al. 2006).

* E-mail: Andrew.Walsh@jcu.edu.au

In the present investigation we have used the Mopra telescope for spectral line mapping of a $5' \times 5'$ region around NGC 6334 I and I(N) throughout the entire 3 mm range.

2 OBSERVATIONS

Observations were carried out in 2006 on June 25th, using the 22m Mopra telescope near Coonabarabran, New South Wales, Australia¹. We used the recently commissioned 3 mm MMIC receiver in combination with the new Mopra spectrometer, MOPS, in broadband mode² resulting in an instantaneous bandwidth of 8 GHz split over four overlapping IFs of 2.2 GHz each. At the time of the observations MOPS provided 1024 channels per IF, giving a total of 8192 channels. The spectral resolution of the observations was 2 MHz corresponding to a velocity resolution of about 6 km s^{-1} per channel. For NGC 6334, this velocity resolution is about the same, or slightly larger than expected line widths, which means while we do not expect to spectrally resolve many lines, we will not suffer a significant loss in signal due to spectral smearing. Thus, this work will necessarily concentrate on morphologies and integrated intensities of emission, rather than any analysis of kinematic structure.

The pointing centre for the maps was chosen to be RA(J2000) = 17 20 54.24, Dec(J2000) = -35 46 11.5, which is approximately half way between NGC 6334 I and I(N). We used the on-the-fly mapping routine to map an area of $5' \times 5'$ around this position. Due to incomplete sampling of the edges of the map, a slightly smaller area is considered in this work. A scanning rate of $3.5 \text{ arcsec s}^{-1}$ was used. Data were averaged every 2 seconds which gives an optimum data collection rate with minimal smearing of the output. A spacing of 10 arcseconds was used between each scanning row. Assuming a beam of between 33 and $36''$, depending on the frequency (Ladd et al. 2005), this observing mode resulted in a fully sampled map. A single map was obtained in about 90 minutes, including about 15% of this time for T_{SYS} calibration, reference observations and pointing on a nearby SiO maser (AH Sco). Poor weather (clouds) affected some of the data, which usually appears as faint horizontal stripes in the data (see the following sections for details).

3 RESULTS

Figure 1 shows spectra at I and I(N) across the 3 mm band. Each spectrum was made by integrating the emission over a box approximately equal to the size of the beam. The spectrum for NGC 6334 I was centred on the methanol maser site that overlaps with the UC H_{II} region (17 20 53.35, -35 47 1.6) and the spectrum for NGC 6334 I(N) was centred on the methanol maser site (17 20 54.58 -35 45 8.6). Across the band, we detect a total of 52 transitions from 19 species. Details of each detection are given in Table 1. For each of

these transitions, we provide a map of the emission, shown in Figure 3.

Figure 2 shows dust continuum emission in the region taken using SCUBA on the JCMT (Göran Sandell, *private communication*). These images were taken on June 26th and July 1st, 1998, with measured half-power beam widths of $14.6''$ at $850 \mu\text{m}$ and $8''$ at $450 \mu\text{m}$. In this Figure, the plus symbols represent the positions of methanol maser emission (Walsh et al. 1998). In the north, the methanol maser site marks the position of NGC 6334 I(N). In the south, two maser sites are seen, spaced about $7''$ apart. Coincident with one of these maser sites, and marked by the diamond is the UC H_{II} region NGC 6334 I. The other, nearby maser site marks the position of a hot core (eg. Beuther et al. 2005). The circle marks the position, and approximate extent of the H_{II} region NGC 6334 E. Strong sources of submm continuum emission appear associated with both NGC 6334 I and NGC 6334 I(N). At the position of NGC 6334 I, the dust continuum appears to peak at the UC H_{II} region position, rather than the hot core located to the north-west. The continuum emission also appears to be essentially unresolved here. Higher resolution observations by Hunter et al. (2006) show the continuum emission does fragment into multiple sources.

The continuum emission associated with NGC 6334 I appears to be extended over almost an arcminute, corresponding to a projected length of nearly 0.5 pc. The continuum emission also appears to peak about $6''$ to the south-east of the maser site associated with NGC 6334 I(N). The greyscale continuum images also show the low level dust emission, which exhibits a prominent filamentary structure running from the south-western corner to the centre-top of the field of view. Other, weaker filamentary structures appear as a bridge between NGC 6334 I and I(N), as well as possibly connecting NGC 6334 I and NGC 6334 E, although very little continuum emission is coincident with the H_{II} region NGC 6334 E. The very weak filamentary structure appears to extend from NGC 6334 I(N) to the north-eastern corner of the field of view. Finally, there is some emission seen directly to the north of NGC 6334 I(N), which may be an extension of the filament seen to bridge the gap between NGC 6334 I and I(N).

4 DISCUSSION

4.1 Morphological analysis

Since the spectral resolution was relatively coarse, we refrain from an analysis of spectrally resolved data-cubes and only show and interpret integrated images of the different molecular species and isotopologues. Furthermore, the angular resolution of the Mopra telescope in the 3 mm band is $\sim 36''$ (at 90 GHz) corresponding to a linear resolution of $\sim 65000 \text{ AU}$ or $\sim 0.3 \text{ pc}$. This spatial resolution is not sufficient to analyze spatial differences within one or the other massive star-forming region. However, it allows us to investigate the molecular global properties, similarities and differences between the different massive star-forming regions present in our field of view. In the following, we will qualitatively describe the global spatial characteristics of the different molecular species and its isotopologues.

¹ For detailed information on the facility visit the Mopra www page at <http://www.narrabri.atnf.csiro.au/mopra/>

² Detailed information on the available receivers and backends can be found online in the "Technical Summary of the Mopra Radiotelescope" available at <http://www.narrabri.atnf.csiro.au/mopra/mopragu.pdf>

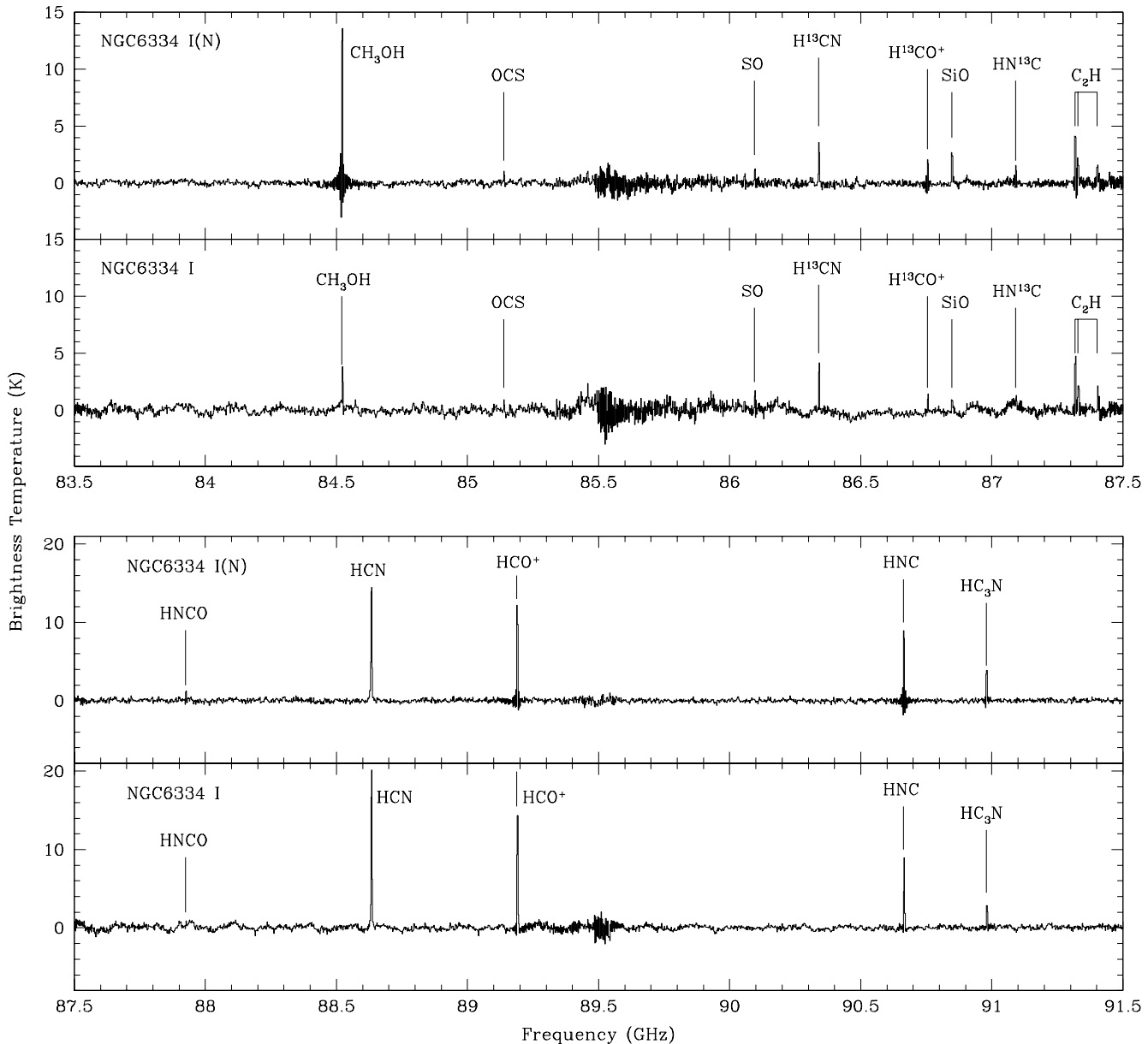


Figure 1. Spectra of NGC 6334 I (lower) and NGC 6334 I(N) (upper) shown between 83.5 and 91.5 GHz. The frequencies of identified lines in each spectrum are indicated with a solid vertical line. Each spectrum was produced by integrating over a square box with each side approximately equal to the beam width ($36''$). Strong lines in the spectrum occasionally produce a ringing artifact close to the line frequency, eg. CH_3OH in I(N). This is a result of the Gibbs phenomenon and is most pronounced with narrow lines, such as masers.

H41 α : The only covered hydrogen recombination line that we could image and is found as expected toward the UCHII region associated with NGC 6334 I.

C₂H: C₂H shows a peculiar spatial morphology since its main emission peak is associated with NGC 6334 I(N) and appears as a weak hole at the position of NGC 6334 E. Furthermore, extended emission closely follows the dust continuum ridge shown in Figure 2. This molecule shows no clear peak toward the southern source NGC 6334 I. The dearth of emission coincident with both NGC 6334 E and I suggests

that this molecule is destroyed close to HII region environments.

Unsaturated hydrocarbons like C₂H are known to be strong at early evolutionary stages (eg. Millar & Nejad 1985; Turner et al. 1999). During the warm-up of the cores it reacts quickly with oxygen to form CO through ion-molecule chemistry (eg. Turner et al. 1999; Herbst & Leung 1986). These models are consistent with our finding of the C₂H peak close to NGC 6334 I(N) and much less emission toward the hot core NGC 6334 I or the HII region NGC 6334 E. Fur-

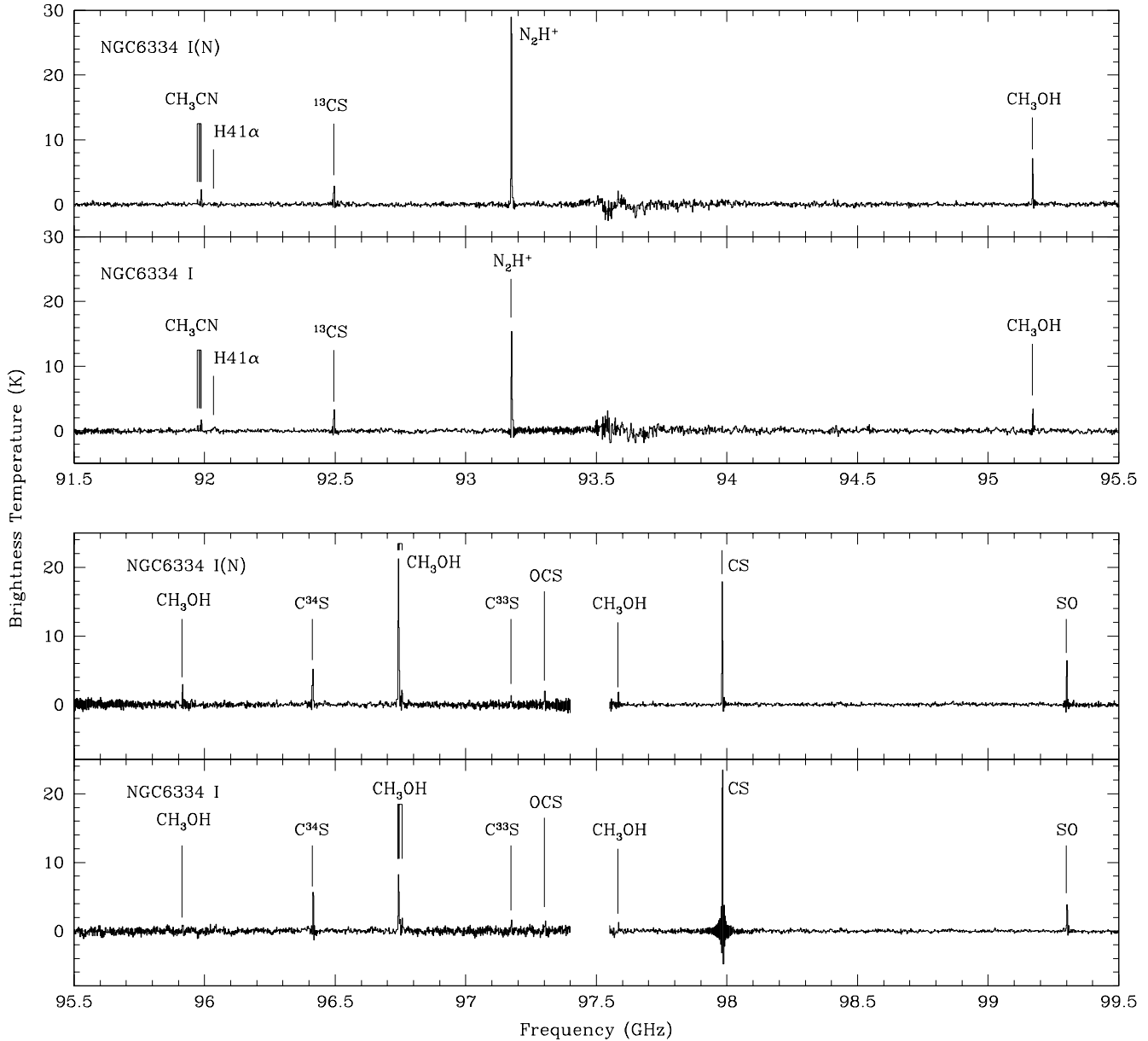


Figure 1 – *continued* ... Frequency range is between 91.5 and 99.5 GHz.

thermore, Beuther et al. (2008) confirm that during ongoing evolution C₂H abundances decrease toward star formation sites. Thus, C₂H is a good tracer of gas that is not directly associated with active star formation.

CN: The radical CN appears to be smoothly distributed over a region covering NGC 6334 I, E and I(N). One transition is slightly stronger at NGC 6334 I, and the other is slightly stronger at NGC 6334 I(N). However, these are weak peaks, over the extended emission and so it is not possible to tell if the difference in relative intensities is real or due to noise variations. CN, like C₂H, appears to be a good tracer of gas not directly associated with active star formation.

¹²CO, ¹³CO, C¹⁸O and C¹⁷O: Carbon monoxide and its isotopologues are easily detected in our field of view. However, the spatial distribution is surprising because it does not trace clearly any of the two main massive star-forming regions, NGC 6334 I or I(N). The main emission peak is located approximately 50'' north-west of NGC 6334 I, closer to the UCHII region NGC 6334 E (but not coincident). We note that this peak does not appear pronounced in any other spectral line imaged in this work, nor does it feature prominently in the dust continuum map. Since only CO (1–0) transitions are prominent at this position (17 20 48.45, -35 46 30) and these transitions have a low effective critical

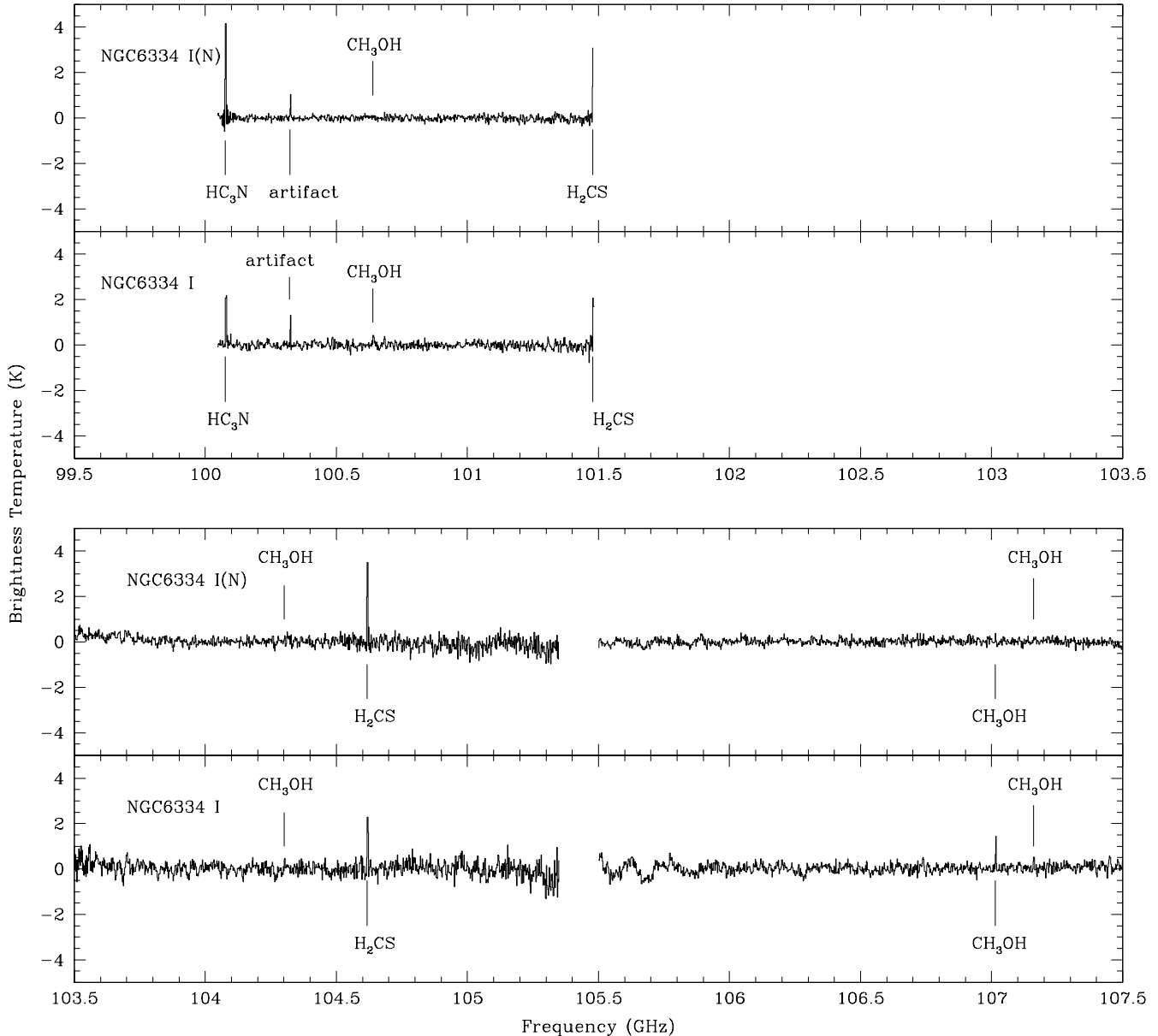


Figure 1 – *continued* ... Frequency range is between 99.5 and 107.5 GHz. The large blank areas shown on the upper plot are because the data in these frequency ranges were unfortunately unusable. Note that one line appears at approximately 100.322 GHz. This is a reflection of HNC at 90.664 GHz, and not a real line.

density ($\sim 10^2 \text{ cm}^{-3}$), we believe this line of sight contains a high column density of low density gas without any significant high density centre that might contain star formation. While ^{12}CO , ^{13}CO and C^{18}O show weaker secondary peaks toward NGC 6334 I and I(N), these are barely detectable in the rarest isotopologue C^{17}O . Based on the mm continuum maps (e.g., Sandell 2000, see also Figure 2) it is obvious that the highest gas column densities are toward NGC 6334 I and I(N), therefore, non-detection of these peaks in rare CO isotopologues cannot be explained by column density effects. The temperatures toward NGC 6334 I and I(N) exceed 100 K

(Beuther et al. 2005) whereas the excitation temperatures of the upper energy levels of the $J = 1 - 0$ carbon monoxide transitions are only of the order 5 K. With a typical Boltzmann distribution, one would expect, for example, the $J = 6 - 5$ transitions to peak closer to the warm regions NGC 6334 I and I(N).

An additional interesting feature in the CO maps is the more extended north-south ridge. It would be useful to have larger maps to investigate to what extent this ridge is continuing, but a comparison with the mm continuum map in-

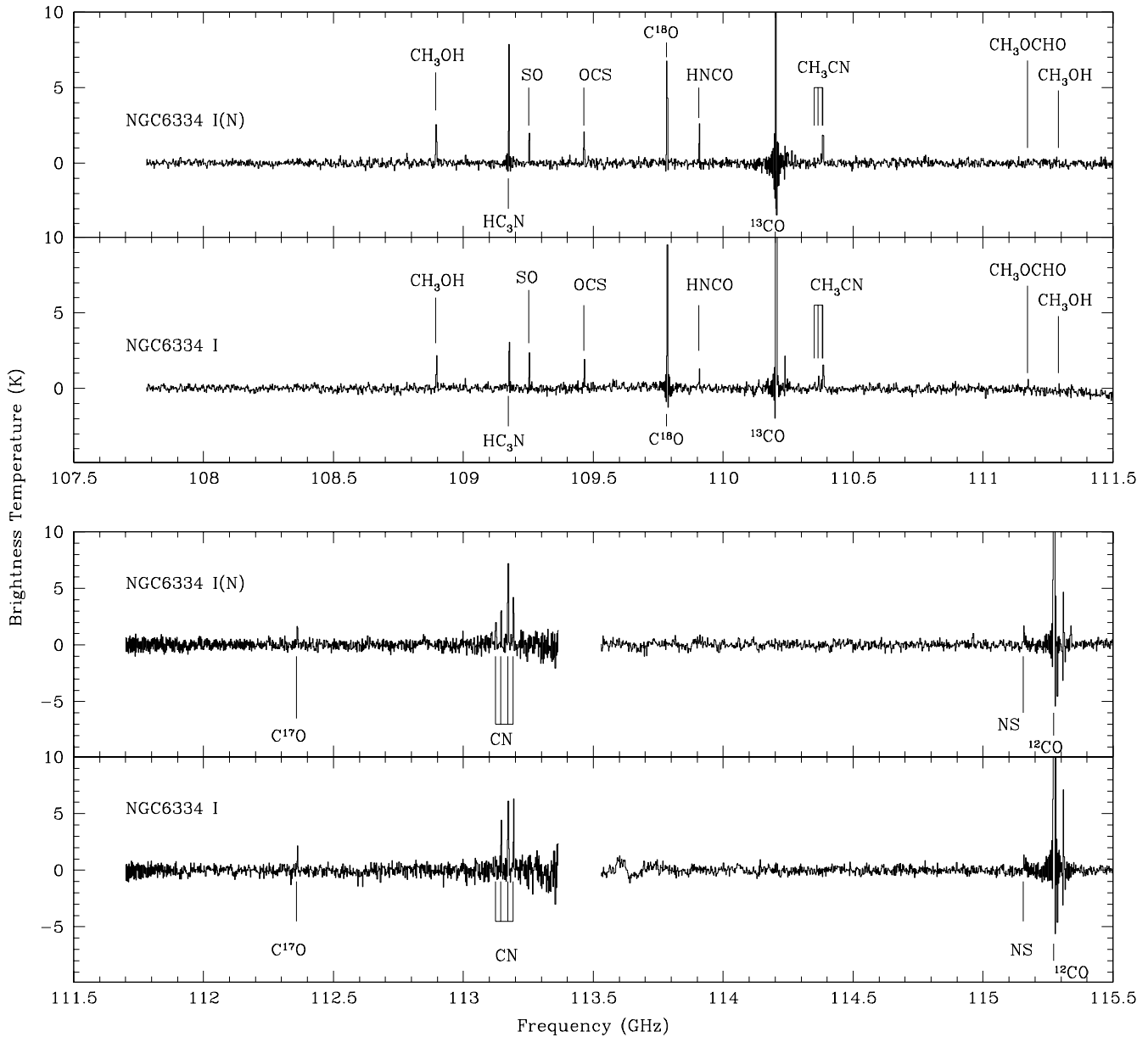


Figure 1 – *continued* ... Frequency range is between 107.5 and 115.5 GHz. The frequencies of identified lines in each spectrum are indicated with a solid vertical line below the spectrum.

indicates that this CO ridge has no direct counterpart in the dense gas and dust component.

N_2H^+ : The well-known tracer of star formation at young evolutionary stages N_2H^+ exhibits its strongest peak toward the northern region NGC 6334 I(N). However, the molecule has additional – although progressively weaker – emission peaks associated with the more evolved region NGC 6334 I. N_2H^+ emission is at a local minimum at the position of NGC 6334 E, indicating that this ion tends to avoid the HII region environment. In addition to this, N_2H^+ clearly shows extended emission, which is positionally co-

incident with the main filament shown in dust continuum emission (Figure 2). Of all the spectral line species covered in this work, N_2H^+ most closely follows the dust continuum emission, showing it to be a good tracer of cold and dense material, including in star forming regions.

HCO^+ and $H^{13}CO^+$: The HCO^+ map clearly shows its main emission peaks associated with the dense cores NGC 6334 I and I(N). It shows an additional secondary peak associated with the main carbon monoxide peaks further to the east, as well as hints of the larger scale north-south ridge discussed for CO and its isotopologues above.

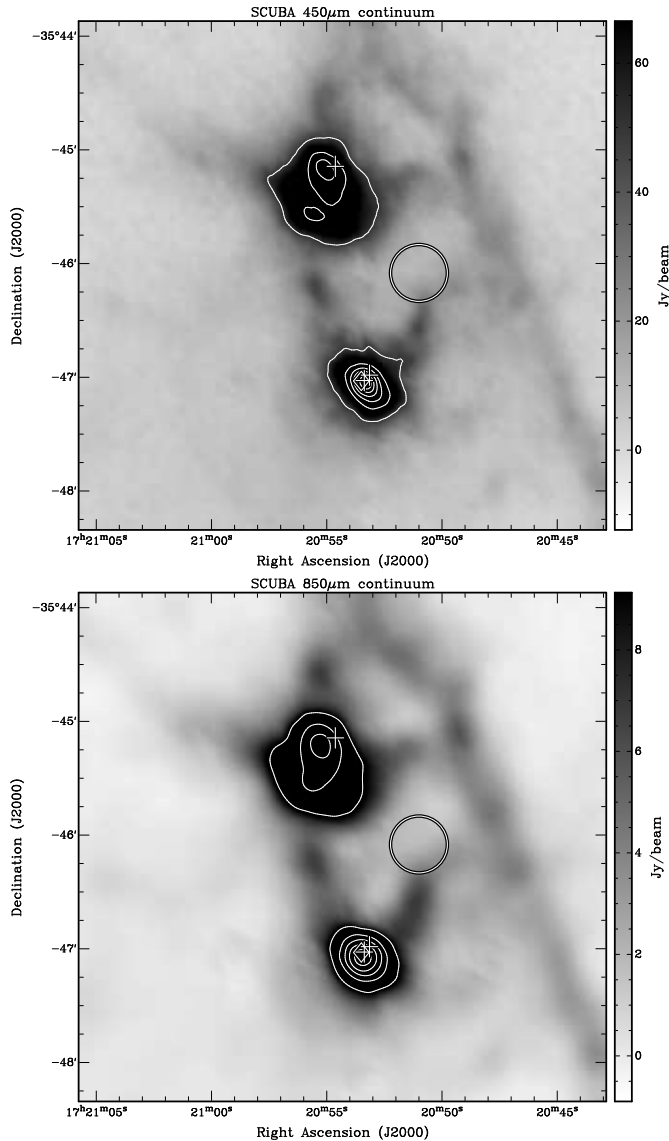


Figure 2. Dust continuum images taken with SCUBA on the JCMT, from Gören Sandell. The large circle represents the approximate size and position of the HII region NGC 6334 E (Carral et al. 2002). The diamond represents the position of the UC HII region NGC 6334 F, also known as NGC 6334 I. The two plus symbols next to the diamond represent the position of two methanol maser sites (Walsh et al. 1998). The single plus symbol in the northern half of each image represents the position of NGC 6334 I(N), traced by a methanol maser site (Walsh et al. 1998). **(top)** 450 μ m image. The lowest contour is at 50 Jy beam⁻¹ and contours are spaced at 50 Jy beam⁻¹. The peak flux density in the map is 369 Jy beam⁻¹. **(bottom)** 850 μ m image. The lowest contour is at 10 Jy beam⁻¹ and contours are spaced at 10 Jy beam⁻¹. The peak flux density in the map is 59 Jy beam⁻¹.

For H¹³CO⁺ we cannot identify the north-south ridge anymore but the other features resemble those of the main isotopologue. It is interesting to note that the main intensity peaks for both isotopologues are associated with NGC 6334 I(N) and not the more prominent hot-core type region NGC 6334 I. This is reminiscent to the HC₃N map published by Sollins & Megeath (2004).

CH₃OH, thermal and class I/II masers: The spectral setup covers many CH₃OH and class I and class II maser lines as shown in Table 1 (see also Müller et al. 2004). It is impossible to definitively claim detection of masers given the current observations with a beam larger than 30'', and a spectral resolution of a few km/s. However, we can comment on the likelihood of any transition showing masing activ-

ity, based on the relative intensities of lines at the positions of I and I(N). It is likely, then, that NGC 6334 I(N) shows maser emission in the Class I transitions at 84.521 GHz and 95.169 GHz, and in the Class II transition at 108.894 GHz. Val'tts et al. (2000) confirms the masing nature of the Class I transition at 95.169 GHz. NGC 6334 I, on the other hand, does not show strong emission in any of the masing transitions, except perhaps the Class II transition at 107.013 GHz. Cragg et al. (2001) and Val'tts et al. (1999) have both observed this Class II transition towards NGC 6334 I and confirm it is a maser.

The thermal methanol transitions appear to divide into two types, based on the strength of their emission. Methanol transitions showing strong emission at 95.914, the quadru-

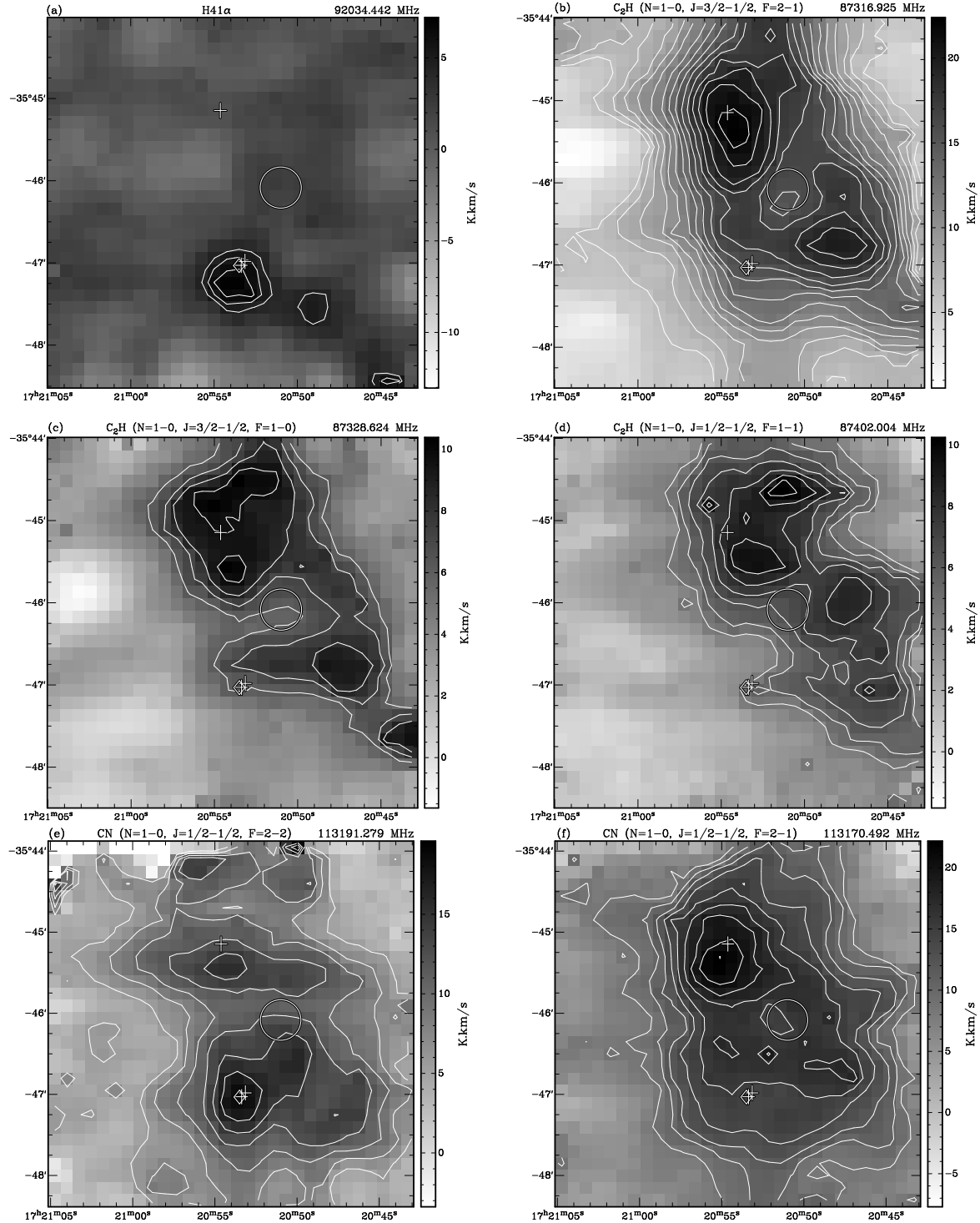


Figure 3. Integrated intensity images and contours for detected transitions. The large circle represents the approximate size and position of the HII region NGC 6334E (Carral et al. 2002). The diamond represents the position of the UC HII region NGC 6334F, also known as NGC 6334I. The two plus symbols next to the diamond represent the position of two methanol maser sites (Walsh et al. 1998). The single plus symbol in the northern half of each image represents the position of NGC 6334I(N), traced by a methanol maser site (Walsh et al. 1998). Axes are labelled in coordinates of Ra and Dec (J2000). The intensity scale is in units of brightness temperature multiplied by velocity. **(a)** H41 α radio recombination line. Contours start at 5σ and increase in 1σ steps, where 1σ is 0.9 K km s^{-1} . **(b)** C₂H (N=1-0, J=3/2-1/2, F=2-1) — ethynyl radical. Contours start at 5σ and increase in 1σ steps, where 1σ is 1.2 K km s^{-1} . **(c)** C₂H (N=1-0, J=3/2-1/2, F=1-0) — ethynyl radical. Contours start at 5σ and increase in 1σ steps, where 1σ is 1.2 K km s^{-1} . **(d)** C₂H (N=1-0, J=1/2-1/2, F=1-1) — ethynyl radical. Contours start at 5σ and increase in 1σ steps, where 1σ is 0.9 K km s^{-1} . **(e)** CN (N=1-0, J=1/2-1/2, F=2-2) — cyanogen radical. Contours start at 5σ and increase in 2σ steps, where 1σ is 1.1 K km s^{-1} . Note that this transition was particularly sensitive to weather. Features in the northern quarter of the image (north of I(N)) are almost certainly a result of poor weather and not real. **(f)** CN (N=1-0, J=1/2-1/2, F=2-1) — cyanogen radical. Contours start at 5σ and increase in 1σ steps, where 1σ is 1.7 K km s^{-1} .

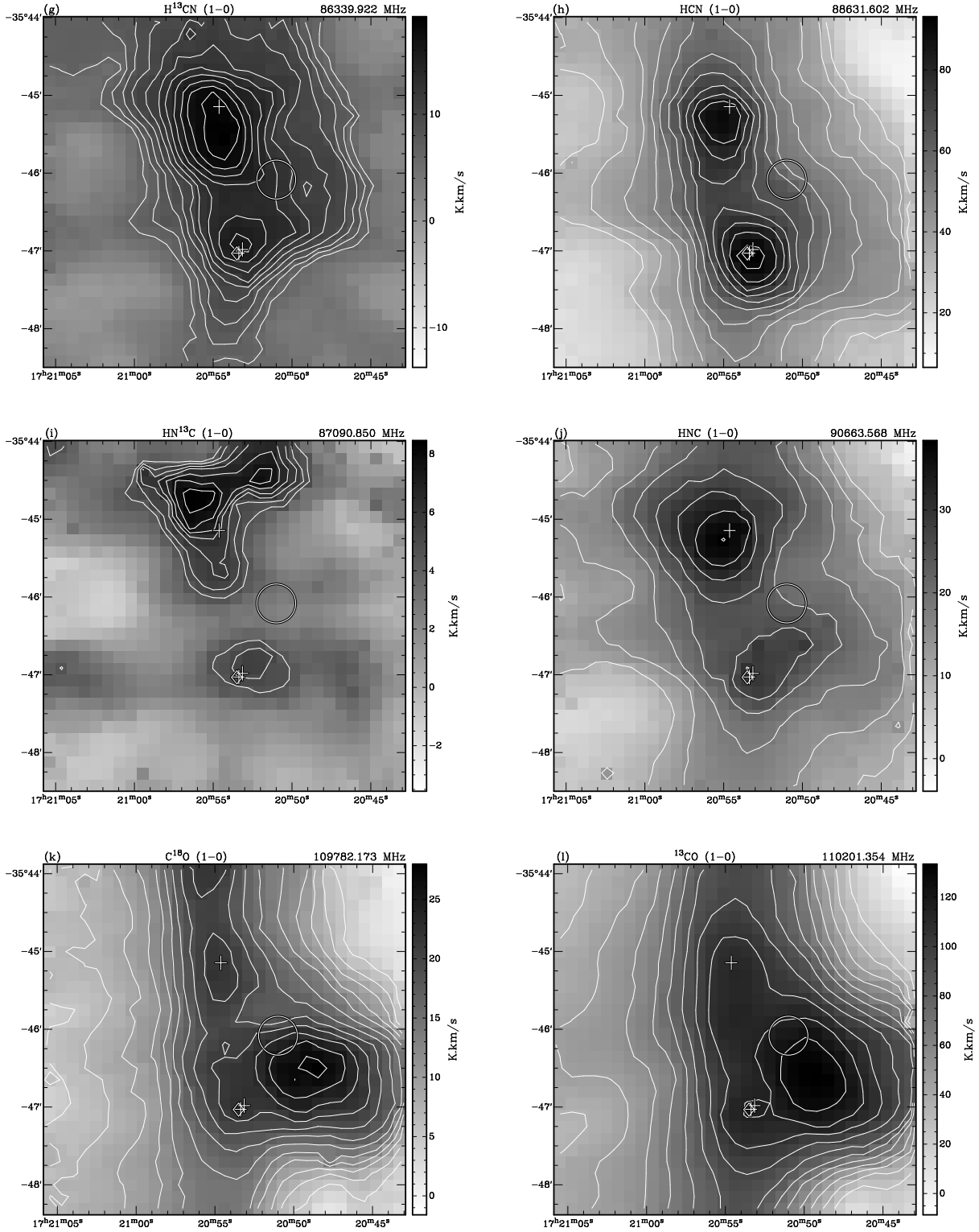


Figure 3 – continued (g) H^{13}CN (1–0) — hydrogen cyanide. Contours start at 5σ and increase in 1σ steps, where 1σ is 1.2 K km s^{-1} . (h) HCN (1–0) — hydrogen cyanide. Contours start at 5σ and increase in 1σ steps, where 1σ is 6.0 K km s^{-1} . (i) HN^{13}C (1–0) — hydrogen isocyanide. Contours start at 5σ and increase in 1σ steps, where 1σ is 0.6 K km s^{-1} . (j) HNC (1–0) — hydrogen isocyanide. Contours start at 5σ and increase in 2σ steps, where 1σ is 2.0 K km s^{-1} . (k) C^{18}O (1–0) — carbon monoxide. Contours start at 5σ and increase in 2σ steps, where 1σ is 1.1 K km s^{-1} . (l) ^{13}CO (1–0) — carbon monoxide. Contours start at 5σ and increase in 2σ steps, where 1σ is 5.0 K km s^{-1} .

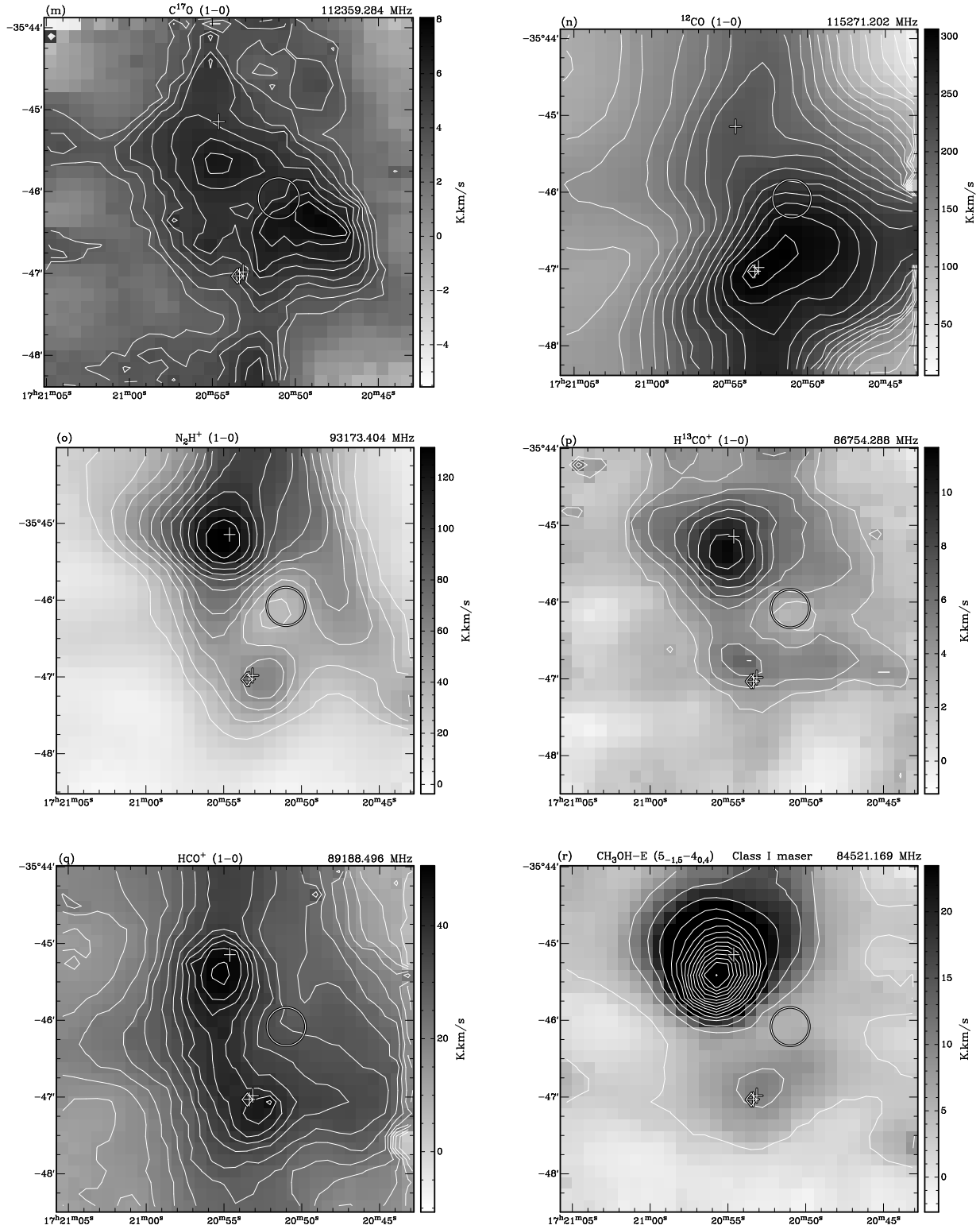


Figure 3 – *continued* (m) C^{17}O (1–0) — carbon monoxide. Contours start at 5σ and increase in 1σ steps, where 1σ is 0.6 K km s^{-1} . (n) ^{12}CO (1–0) — carbon monoxide. Contours start at 5σ and increase in 3σ steps, where 1σ is 5.0 K km s^{-1} . (o) N_2H^+ (1–0) — diazenylium. Contours start at 5σ and increase in 2σ steps, where 1σ is 5.0 K km s^{-1} . (p) H^{13}CO^+ (1–0) — oxomethylum. Contours start at 5σ and increase in 2σ steps, where 1σ is 0.6 K km s^{-1} . (q) HCO^+ (1–0) — oxomethylum. Contours start at 5σ and increase in 2σ steps, where 1σ is 1.6 K km s^{-1} . (r) $\text{CH}_3\text{OH-E}$ ($5_{-1,5} - 4_{0,4}$) — methanol. Contours start at 5σ and increase in 10σ steps, where 1σ is 0.6 K km s^{-1} . This methanol transition is a Class I maser (Müller et al. 2004).

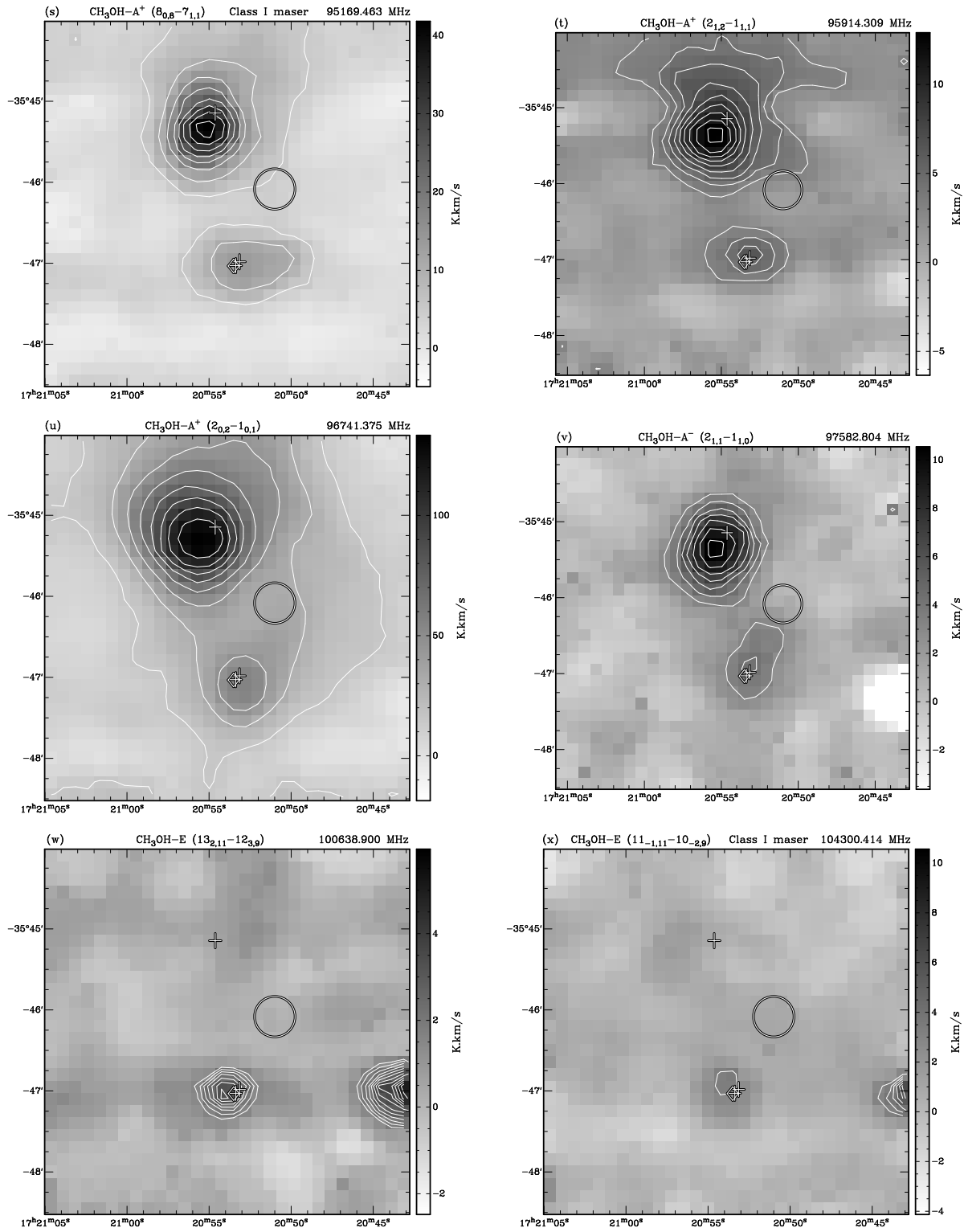


Figure 3 – continued (s) $\text{CH}_3\text{OH-A}^+ (8_{0,8}-7_{1,1})$ — methanol. Contours start at 5σ and increase in 5σ steps, where 1σ is 1.0 K km s^{-1} . This methanol transition is a Class I maser (Müller et al. 2004). (t) $\text{CH}_3\text{OH-A}^+ (2_{1,2}-1_{1,1})$ — methanol. Contours start at 5σ and increase in 2σ steps, where 1σ is 0.6 K km s^{-1} . (u) $\text{CH}_3\text{OH-A}^+ (2_{0,2}-1_{0,1})$ — methanol. Contours start at 5σ and increase in 5σ steps, where 1σ is 3.0 K km s^{-1} . (v) $\text{CH}_3\text{OH-A}^- (2_{1,1}-1_{1,0})$ — methanol. Contours start at 5σ and increase in 2σ steps, where 1σ is 0.6 K km s^{-1} . (w) $\text{CH}_3\text{OH-E} (13_{2,11}-12_{3,9})$ — methanol. Contours start at 5σ and increase in 1σ steps, where 1σ is 0.3 K km s^{-1} . Strong “emission” is seen on the right hand edge of the image, at a declination of approximately $-35^\circ 47'$, which is due to a bad data point, and is not real emission. (x) $\text{CH}_3\text{OH-E} (11_{-1,11}-10_{-2,9})$ — methanol. Contours start at 5σ and increase in 1σ steps, where 1σ is 0.6 K km s^{-1} . This methanol transition is a Class I maser (Müller et al. 2004). “Emission” is seen on the right hand edge of the image, at a declination of approximately $-35^\circ 47'$, which is due to a bad data point, and is not real emission.

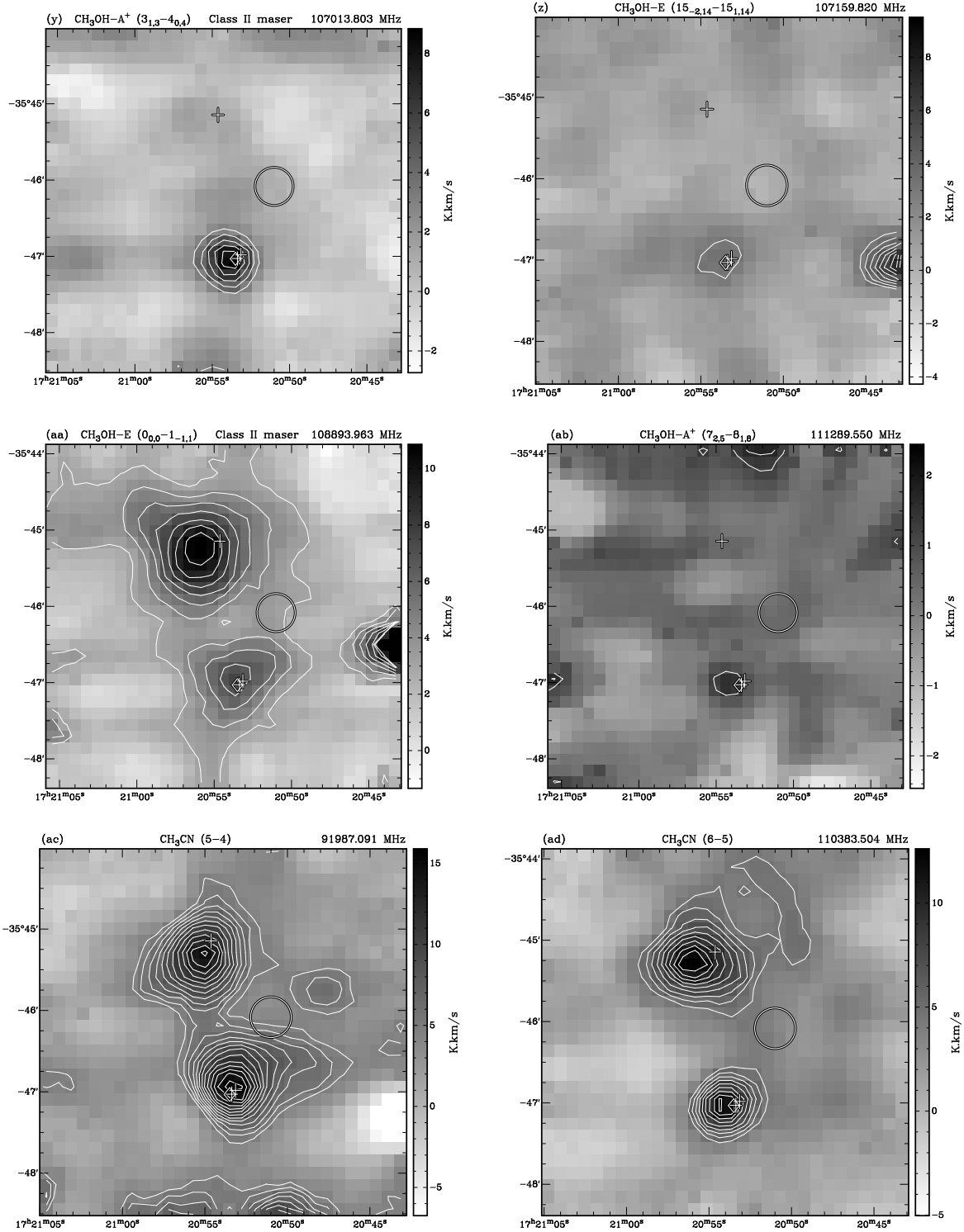


Figure 3 – continued (y) CH₃OH-A⁺ (3_{1,3}-4_{0,4}) — methanol. Contours start at 5 σ and increase in 2 σ steps, where 1 σ is 0.6 K km s⁻¹. This methanol transition is a Class II maser (Müller et al. 2004). (z) CH₃OH-E (15_{-2,14}-15_{1,14}) — methanol. Contours start at 5 σ and increase in 1 σ steps, where 1 σ is 0.6 K km s⁻¹. Strong “emission” is seen on the right hand edge of the image, at a declination of approximately -35°47', which is due to a bad data point, and is not real emission. (aa) CH₃OH-E (0_{0,0}-1_{-1,1}) — methanol. Contours start at 5 σ and increase in 2 σ steps, where 1 σ is 0.6 K km s⁻¹. This methanol transition is a Class II maser (Müller et al. 2004). Strong “emission” is seen on the right hand edge of the image, at a declination of approximately -35°46'30'', which is due to a bad data point, and is not real emission. (ab) CH₃OH-A⁺ (7_{2,5}-8_{1,8}) — methanol. Contours start at 3 σ and increase in 1 σ steps, where 1 σ is 0.5 K km s⁻¹. (ac) CH₃CN (5-4) — methyl cyanide. The emission includes all transitions in the K ladder from 0 to 3, inclusive. Contours start at 5 σ and increase in 1 σ steps, where 1 σ is 0.9 K km s⁻¹. We attribute the “emission” seen south of -35°48' to be due to poor weather and is thus not real. (ad) CH₃CN (6-5) — methyl cyanide. The emission includes all transitions in the K ladder from 0 to 3, inclusive. Contours start at 5 σ and increase in 1 σ steps, where 1 σ is 0.9 K km s⁻¹.

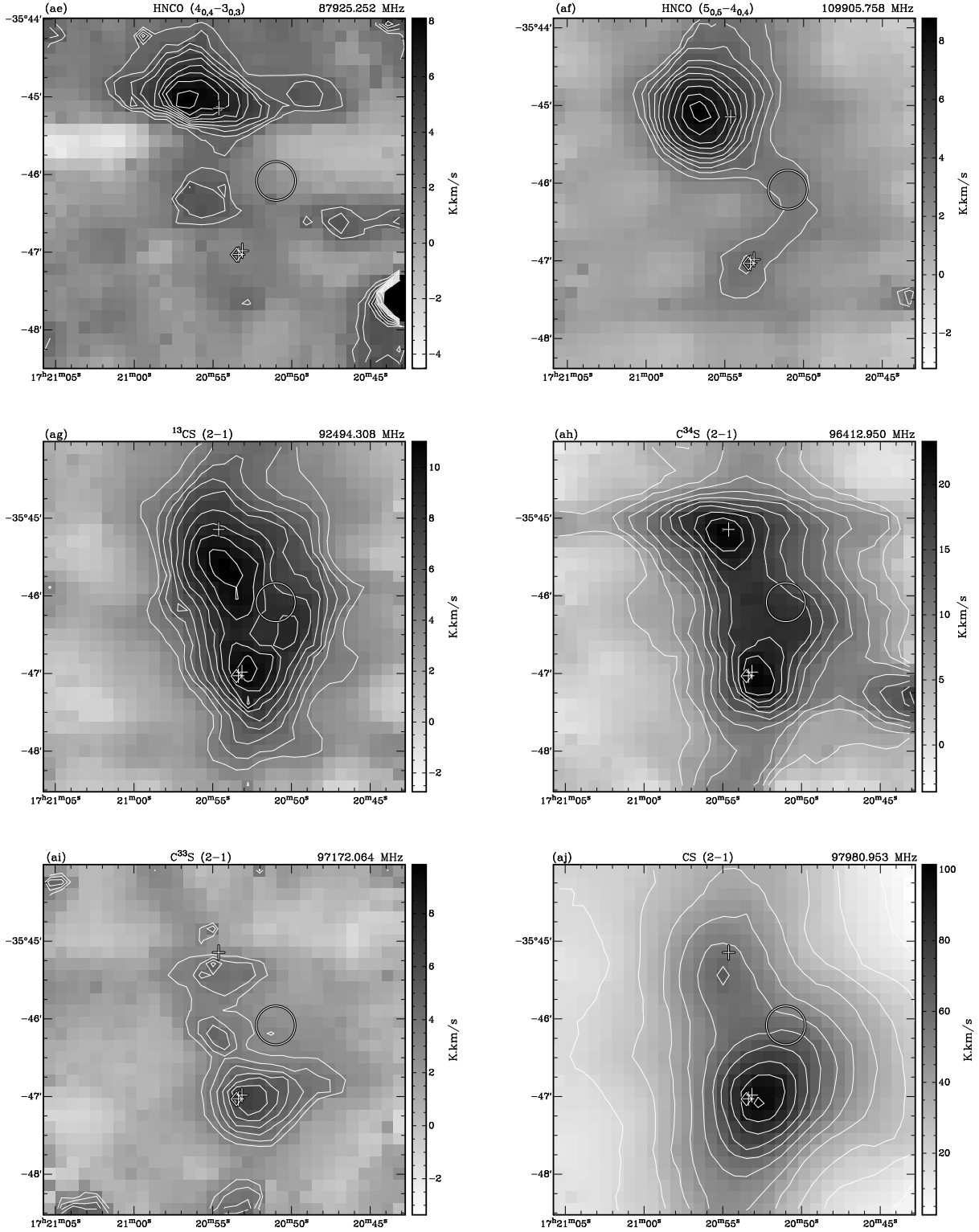


Figure 3 – *continued* (ae) HNC ($4_{0,4}-3_{0,3}$) — isocyanic acid. Contours start at 5σ and increase in 1σ steps, where 1σ is 0.6 K km s^{-1} . Strong “emission” is seen on the right hand edge of the image, at a declination of approximately $-35^{\circ}47'30''$, which is due to a bad data point, and is not real emission. (af) HNC ($5_{0,5}-4_{0,4}$) — isocyanic acid. Contours start at 5σ and increase in 1σ steps, where 1σ is 0.6 K km s^{-1} . (ag) ^{13}CS (2–1) — carbon sulfide. Contours start at 5σ and increase in 1σ steps, where 1σ is 0.7 K km s^{-1} . (ah) C^{34}S (2–1) — carbon sulfide. Contours start at 5σ and increase in 2σ steps, where 1σ is 1.0 K km s^{-1} . Strong “emission” is seen on the right hand edge of the image, at a declination of approximately $-35^{\circ}47'15''$, which is due to a bad data point, and is not real emission. (ai) C^{33}S (2–1) — carbon sulfide. Contours start at 5σ and increase in 1σ steps, where 1σ is 0.6 K km s^{-1} . (aj) CS (2–1) — carbon sulfide. Contours start at 5σ and increase in 5σ steps, where 1σ is 1.8 K km s^{-1} .

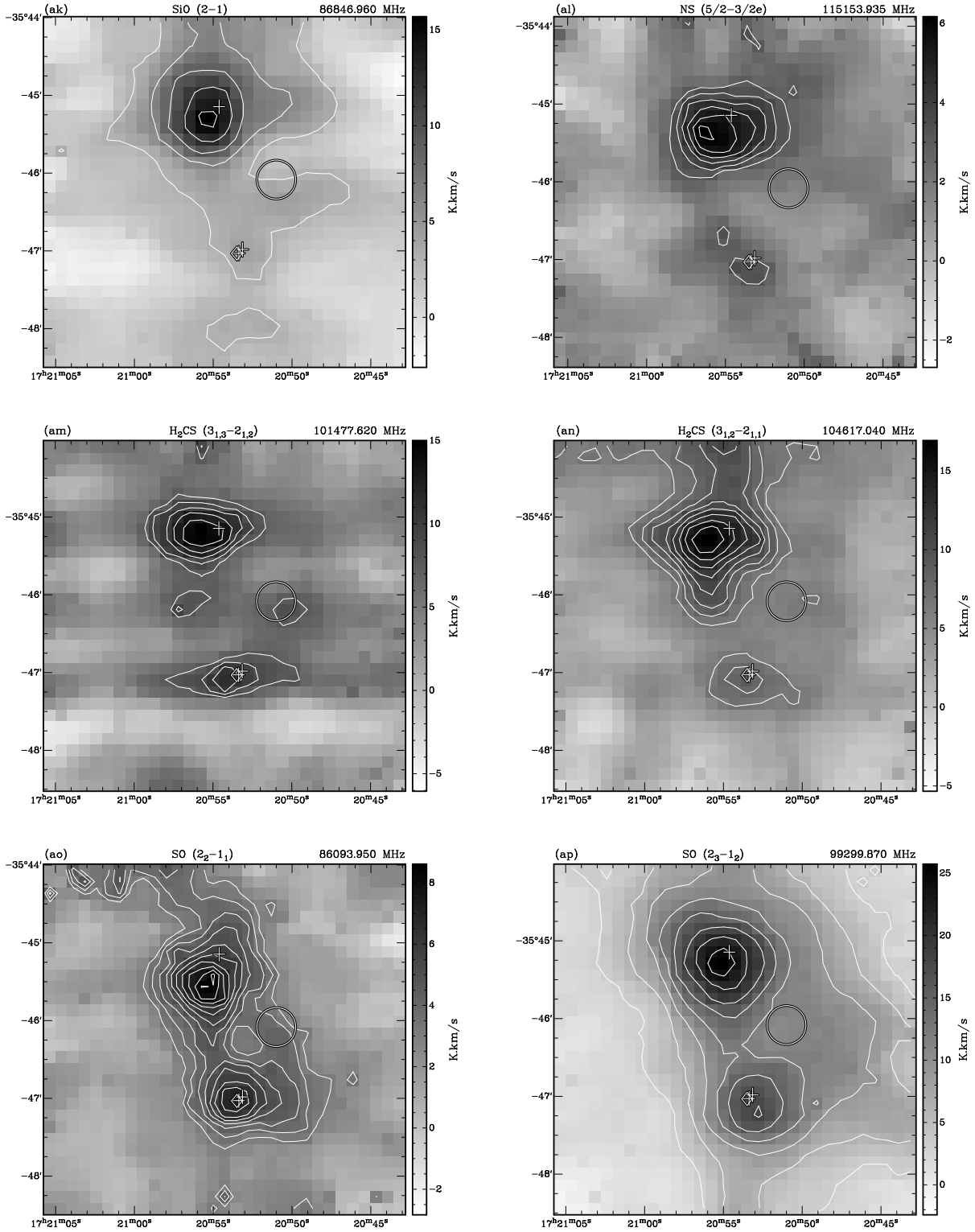


Figure 3 – *continued* (ak) SiO (2-1) — silicon monoxide. Contours start at 5σ and increase in 5σ steps, where 1σ is 0.6 K km s^{-1} . (al) NS (5/2-3/2e) — nitrogen sulfide. Contours start at 5σ and increase in 1σ steps, where 1σ is 0.6 K km s^{-1} . (am) H₂CS (3_{1,3}-2_{1,2}) — thioformaldehyde. Contours start at 5σ and increase in 1σ steps, where 1σ is 1.5 K km s^{-1} . (an) H₂CS (3_{1,2}-2_{1,1}) — thioformaldehyde. Contours start at 5σ and increase in 1σ steps, where 1σ is 1.3 K km s^{-1} . (ao) SO (2₂-1₁) — sulfur monoxide. Contours start at 5σ and increase in 1σ steps, where 1σ is 0.6 K km s^{-1} . (ap) SO (2₃-1₂) — sulfur monoxide. Contours start at 5σ and increase in 5σ steps, where 1σ is 0.6 K km s^{-1} .

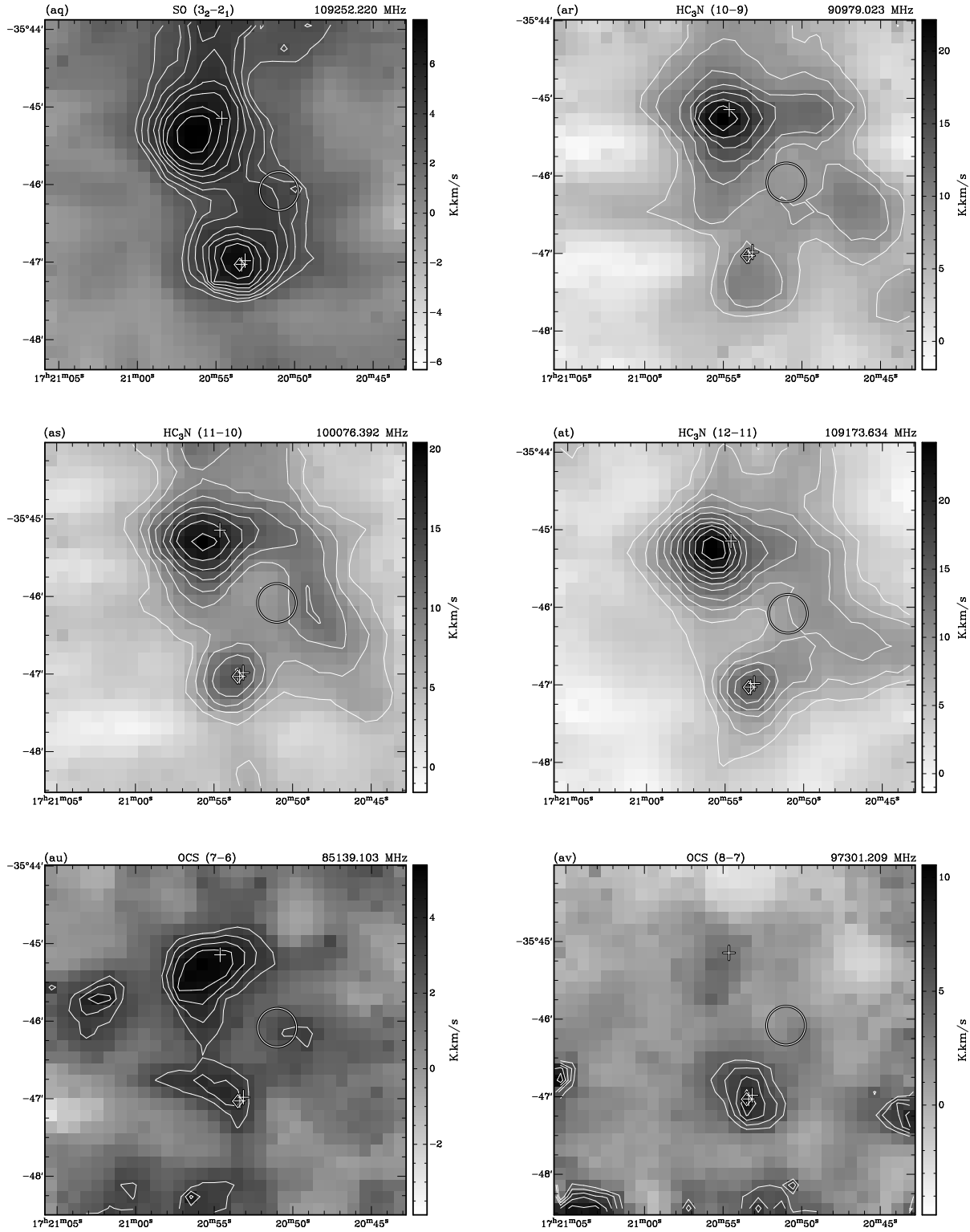


Figure 3 – *continued* **(aq)** SO (3₂–2₁) — sulfur monoxide. Contours start at 5σ and increase in 1σ steps, where 1σ is 0.6 K km s^{-1} . **(ar)** HC₃N (10–9) — cyanoacetylene. Contours start at 5σ and increase in 2σ steps, where 1σ is 1.2 K km s^{-1} . **(as)** HC₃N (11–10) — cyanoacetylene. Contours start at 5σ and increase in 2σ steps, where 1σ is 1.1 K km s^{-1} . **(at)** HC₃N (12–11) — cyanoacetylene. Contours start at 5σ and increase in 2σ steps, where 1σ is 1.1 K km s^{-1} . **(au)** OCS (7–6) — carbonyl sulfide. Contours start at 5σ and increase in 1σ steps, where 1σ is 0.6 K km s^{-1} . **(av)** OCS (8–7) — carbonyl sulfide. Contours start at 5σ and increase in 1σ steps, where 1σ is 1.1 K km s^{-1} . Strong “emission” is seen around edges of the bottom half of the image, which is most likely due to poor weather, and is not real emission.

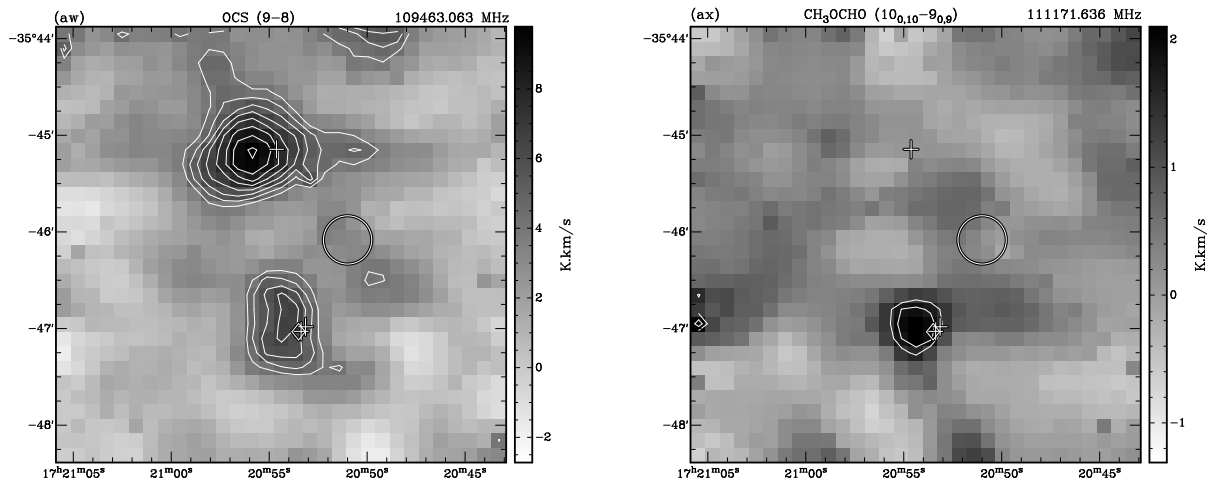


Figure 3 – *continued* (aw) OCS (9–8) — carbonyl sulfide. Contours start at 5σ and increase in 1σ steps, where 1σ is 0.7 K km s^{-1} . “Emission” is seen around the northern edge of the image, which is most likely due to poor weather, and is not real emission. (ax) $\text{CH}_3\text{OCHO-A}$ ($10_{0,10}-9_{0,9}$) — methyl formate. Contours start at 5σ and increase in 1σ steps, where 1σ is 0.3 K km s^{-1} .

plet at 96.7 and at 97.583 GHz all exhibit the bulk of their emission from NGC 6334 I(N). The methanol transitions at 100.639, 107.160 and 111.290 GHz all show weak emission that is only detected towards NGC 6334 I.

CH_3CN : Methyl cyanide is detected in the rotational transitions $J = 5_K - 4_K$ and $6_K - 5_K$. Both integrated intensity maps show two comparably strong peaks toward NGC 6334 I and I(N). Methyl cyanide is potentially useful for temperature estimates, by comparing intensity ratios of components in the K -ladders (Thorwirth et al. 2003). However, the low spectral resolution of these data do not allow us to distinguish individual K -ladder elements. Of all the species mapped in this work, CH_3CN appears to be the one that is most concentrated towards the two regions of active star formation: NGC 6334 I and NGC 6334 I(N).

^{12}CS , ^{13}CS , C^{34}S and C^{33}S : Carbon sulfide shows an interesting spatial variation going from the main isotopologue CS step by step through the rarer isotopologues ^{13}CS and C^{34}S to C^{33}S . While the former main isotopologue peaks toward the southern hot core region NGC 6334 I, the northern peak NGC 6334 I(N) is of comparable brightness for ^{13}CS and C^{34}S . This is likely due to the main CS isotopologue being optically thick, which is then tracing a warmer environment around NGC 6334 I. The optically thin tracers ^{13}CS and C^{34}S show approximately equal brightnesses in I and I(N), suggesting the amount of CS is approximately equal in each. However, the rare isotopologue C^{33}S is brighter in I. We would expect C^{33}S to look similar to ^{13}CS and C^{34}S . This surprising result needs to be investigated further.

SO, OCS, H_2CS and NS: Several sulfur-bearing species have been observed, and all of them show two peaks associated with NGC 6334 I and I(N). The general trend appears to be that the emission is stronger towards NGC 6334 I(N), rather than I. The one exception to this rule is OCS (8-7), where very little emission is detected towards NGC 6334 I(N), even though NGC 6334 I shows a bright peak. This is an unexpected result, especially in light

of the fact that the two other OCS transitions clearly show NGC 6334 I(N) as a strong source of OCS emission.

HC_3N , HNC, HNC, HN^{13}C , HCN, H^{13}CN : There are several hydrogen-carbon-nitrogen chain molecules observed, and all of them show two strong peaks associated with NGC 6334 I and I(N). Except for HCN where the two peaks are of approximately the same strength, in all other lines the region I(N) is clearly the dominant one. For HC_3N this has already previously been reported by Sollins & Megeath (2004). HC_3N is unusual in that it shows extended emission which appears to follow the main filament seen in dust continuum emission (Figure 2), to the west of NGC 6334 E. Furthermore, the HC_3N emission appears to surround NGC 6334 E, but very little emission is seen inside the ring denoting the extent of this H II region. Since its morphology closely resembles that of the dust continuum emission, we find that HC_3N is a good tracer of quiescent, dense gas, as is the case for N_2H^+ .

SiO: As previously reported by Megeath & Tieftrunk (1999), SiO emission is found strongly toward NGC 6334 I(N) and is weaker elsewhere in the field of view. In NGC 6334 I(N) the SiO emission is clearly associated with its molecular outflow(s) (Megeath & Tieftrunk 1999, Hunter et al. in prep.). Previous observations of the G333 giant molecular cloud Lo et al. (2007) have found SiO emission from a region that shows similar properties to NGC 6334 I(N) with an outflow associated with a very early stage of high mass star formation.

CH_3OCHO : The dense core tracing molecule methyl formate is detected only toward the southern hot core region NGC 6334 I.

4.2 Comparison of NGC 6334 I and I(N)

In §4.1, we described the morphology of emission for molecules, or groups of molecules. Here we synthesise this information to present a comparison of the two star forming sites NGC 6334 I and I(N). Based on previous work on this

Table 1. Molecular lines mapped towards the NGC 6334 I(N) region in the present study. Transition frequencies (MHz) were taken from the CDMS (Müller et al. 2001, 2005) in most cases and the JPL catalogue (Pickett et al. 1998). Also given are the integrated intensities for each transition, as measured at NGC 6334 I and I(N) by integrating the emission over one beam, as was done for the spectra presented in Figure 1. 3σ -upper limits are given for those transitions not detected.

Molecule	Transition	Frequency (MHz)	Methanol Maser Class	Integrated Intensity (K km/s)	
				NGC 6334 I	NGC 6334 I(N)
H	41 α	92034.442		26	< 10 ^a
C ₂ H	$N = 1 - 0, J = 3/2 - 1/2, F = 2 - 1$	87316.898		66	60
C ₂ H	$N = 1 - 0, J = 3/2 - 1/2, F = 1 - 0$	87328.585		38	32
C ₂ H	$N = 1 - 0, J = 1/2 - 1/2, F = 1 - 1$	87401.989		35 ^b	23 ^b
CN	$N = 1 - 0, J = 1/2 - 1/2, F = 1/2 - 1/2$	113123.370		8.9	19
CN	$N = 1 - 0, J = 1/2 - 1/2, F = 1/2 - 3/2$	113144.157		38	34
CN	$N = 1 - 0, J = 1/2 - 1/2, F = 3/2 - 1/2$	113170.492		61	64
CN	$N = 1 - 0, J = 1/2 - 1/2, F = 3/2 - 3/2$	113191.279		56	46
H ¹³ CN	$J = 1 - 0$	86339.922		61	57
HCN	$J = 1 - 0$	88631.602		350	300
HN ¹³ C	$J = 1 - 0$	87090.850		19	20
HNC	$J = 1 - 0$	90663.568		100	110
C ¹⁸ O	$J = 1 - 0$	109782.173		69	69
¹³ CO	$J = 1 - 0$	110201.354		360	350
C ¹⁷ O	$J = 1 - 0$	112359.284		19	21
¹² CO	$J = 1 - 0$	115271.202		930	680
N ₂ H ⁺	$J = 1 - 0$	93173.392		210	440
H ¹³ CO ⁺	$J = 1 - 0$	86754.288		16	24
HCO ⁺	$J = 1 - 0$	89188.525		170	150
CH ₃ OH- <i>E</i>	$J_{K_a, K_c} = 5_{-1,5} - 4_{0,4}$	84521.169	I	80	180
CH ₃ OH- <i>A</i> ⁺	$J_{K_a, K_c} = 8_{0,8} - 7_{1,7}$	95169.463	I	41	88
CH ₃ OH- <i>A</i> ⁺	$J_{K_a, K_c} = 2_{1,2} - 1_{1,1}$	95914.309		16	32
CH ₃ OH- <i>A</i> ⁺	$J_{K_a, K_c} = 2_{0,2} - 1_{0,1}$	96741.375		150	370
CH ₃ OH- <i>A</i> ⁻	$J_{K_a, K_c} = 2_{1,1} - 1_{1,0}$	97582.804		9.5	24
CH ₃ OH- <i>E</i>	$J_{K_a, K_c} = 13_{2,11} - 12_{3,9}$	100638.900		4.9	< 0.9 ^a
CH ₃ OH- <i>E</i>	$J_{K_a, K_c} = 11_{-1,11} - 10_{-2,9}$	104300.414	I	5.5	< 1.8 ^a
CH ₃ OH- <i>A</i> ⁺	$J_{K_a, K_c} = 3_{1,3} - 4_{0,4}$	107013.803	II	15	2.7
CH ₃ OH- <i>E</i>	$J_{K_a, K_c} = 15_{-2,14} - 15_{1,14}$	107159.820		8.2	< 1.8 ^a
CH ₃ OH- <i>E</i>	$J_{K_a, K_c} = 0_{0,0} - 1_{-1,1}$	108893.963	II	18	28
CH ₃ OH- <i>A</i> ⁺	$J_{K_a, K_c} = 7_{2,5} - 8_{1,8}$	111289.550		1.9	< 1.2 ^a
CH ₃ CN	$J_K = 5_0 - 4_0$	91987.091		41 ^c	35 ^c
CH ₃ CN	$J_K = 5_1 - 4_1$	91985.318			
CH ₃ CN	$J_K = 5_2 - 4_2$	91979.998			
CH ₃ CN	$J_K = 5_3 - 4_3$	91971.134			
CH ₃ CN	$J_K = 6_0 - 5_0$	110383.504		30 ^d	32 ^d
CH ₃ CN	$J_K = 6_1 - 5_1$	110381.376			
CH ₃ CN	$J_K = 6_2 - 5_2$	110374.993			
CH ₃ CN	$J_K = 6_3 - 5_3$	110364.358			
HNCO	$J_{K_a, K_c} = 4_{0,4} - 3_{0,3}$	87925.237		< 1.8 ^a	25
HNCO	$J_{K_a, K_c} = 5_{0,5} - 4_{0,4}$	109905.749		12	23
¹³ CS	$J = 2 - 1$	92494.308		36	32
C ³⁴ S	$J = 2 - 1$	96412.950		73	61
C ³³ S	$J = 2 - 1$	97172.064		21	14
CS	$J = 2 - 1$	97980.953		290	210
SiO	$J = 2 - 1$	86846.960		13	41
NS	² Π _{1/2} N=2-1, J=5/2-3/2 F=7/2-5/2, c-state	115153.835		8.5	17

^a 3σ -upper limit

^b blend with C₂H $N = 1 - 0, J = 1/2 - 1/2, F = 0 - 1$ at 87407.165 MHz

^c Integrated emission for all $J = 5 - 4$ transitions

^d Integrated emission for all $J = 6 - 5$ transitions

Table 1 – *continued*

Molecule	Transition	Frequency (MHz)	Methanol Maser Class	Integrated Intensity (K km/s)	
				NGC 6334 I	NGC 6334 I(N)
H ₂ CS	$J_{K_a, K_c} = 3_{1,3} - 2_{1,2}$	101477.810		>24	>20
H ₂ CS	$J_{K_a, K_c} = 3_{1,2} - 2_{1,1}$	104617.040		27	34
SO	$N_J = 2_2 - 1_1$	86093.950		22	19
SO	$N_J = 2_3 - 1_2$	99299.870		53	69
SO	$N_J = 3_2 - 2_1$	109252.220		18	21
HC ₃ N	$J = 10 - 9$	90979.023		38	48
HC ₃ N	$J = 11 - 10$	100076.392		27	38
HC ₃ N	$J = 12 - 11$	109173.634		33	59
OCS	$J = 7 - 6$	85139.103		12	17
OCS	$J = 8 - 7$	97301.209		19	19
OCS	$J = 9 - 8$	109463.063		19	25
CH ₃ OCHO ^e	$J_{K_a, K_c} = 10_{0,10} - 9_{0,9}$	111171.636		4.5	< 0.9 ^a

^e Blend of A and E types

region (eg. Walsh et al. 1998), it is clear that NGC 6334 I appears to be more evolved than I(N): it contains a prominent UC HII region, as well as a strong infrared source, whereas only weak radio continuum (Rodríguez et al. 2007) and infrared emission (Walsh et al. 1999) has been found in the vicinity of I(N). We also find evidence for an evolutionary difference in our data. Both the CS/N₂H⁺ and CS/HNCO ratios are much larger for NGC 6334 I than for I(N). Previous work on the CS/N₂H⁺ ratio (Zinchenko, Caselli & Pirogov 2009) and CS/HNCO ratio (Martín et al. 2008) have indicated that CS is likely to be enhanced in abundance towards photodissociation regions (PDRs), whilst both N₂H⁺ and HNCO are likely to be reduced in abundance towards PDRs. Thus, NGC 6334 I shows PDR-like ratios, presumably due to the UC HII region, whereas abundances of both N₂H⁺ and HNCO do not appear to be reduced, compared to CS in NGC 6334 I(N), where a PDR is yet to form.

When comparing the non-masing lines of CH₃OH, we find that the emission is stronger towards NGC 6334 I in the 100.638, 107.159 and 111.289 GHz transitions. CH₃OH emission is stronger towards NGC 6334 I(N) in the 95.915, 96.741 (quadruplet) and 97.582 GHz transitions. The stronger transitions in NGC 6334 I all have upper energy levels between 103 and 304 K, whilst all the stronger transitions in NGC 6334 I(N) have upper energy levels no greater than 22 K. Thus, we can attribute the stronger emission in NGC 6334 I to hot CH₃OH and the stronger emission in NGC 6334 I(N) to cold CH₃OH emission. Whilst previous work has shown that both NGC 6334 I and I(N) have hot components, with temperatures in excess of 400 K (Beuther et al. 2007), it is clear that the large-scale CH₃OH observed here has only had time to heat up in NGC 6334 I.

We detect CH₃OCHO only towards NGC 6334 I. This molecule is thought to be produced only after a young star or protostar has heated up the surrounding material to above 100 K (Garrod & Herbst 2006). This provides further evidence of the more evolved state of NGC 6334 I over that of I(N).

4.3 Line ratio maps

The ratio of integrated intensities for different spectral lines can potentially be used to identify physical and chemical characteristics of regions within the map. For example, a simple comparison of ratios for different lines of the same species might be used to map physical quantities such as density and temperature. However, most species detected in multiple spectral lines (ie. CN, CH₃CN, HNCO, SO, HC₃N and OCS) show only a narrow range of energy levels over the multiple spectral lines. Thus only small changes in line ratios are expected from different spectral lines of the same species. In addition to this, small differences in the relative position of maps made at different frequencies can lead to artifacts that can dominate line ratios. In the present study, these complicating factors make such line ratio maps too unreliable to interpret. The only exception to this is CH₃OH, where clear differences in the intensities of lines are seen between NGC 6334 I and I(N), as discussed in §4.1.

It is possible to compare line ratios between species, that have been observed simultaneously, as this eliminates any relative positional offsets, as well as any varying effects of weather. In Figure 4, we show images based on the ratio of line integrated intensities for different species.

The upper-left image shows the C¹⁸O/¹²CO line ratio map. The greatest ratio is found surrounding NGC 6334 I(N). A high ratio between these two lines means that the ¹²CO line is optically thick. We also see a secondary peak in the ratio to the south-west of NGC 6334 E, which is close to the peak ¹²CO peak integrated intensity (shown in contours). At this position, it is likely that there is a high column density of gas. At NGC 6334 I, the line ratio is relatively low. The ¹²CO gas is likely optically thick here since it is one of the centres of high column density gas in many other lines. The relatively low ratio, compared to that found in NGC 6334 I(N) indicates that the ¹²CO emission is likely to be optically thick along most lines of sight covered in these observations.

The upper-right image shows the HNCO/C¹⁸O line ratio map. As mentioned in §4.2, HNCO tends to be destroyed in PDRs. Thus, the line ratio map broadly shows two re-

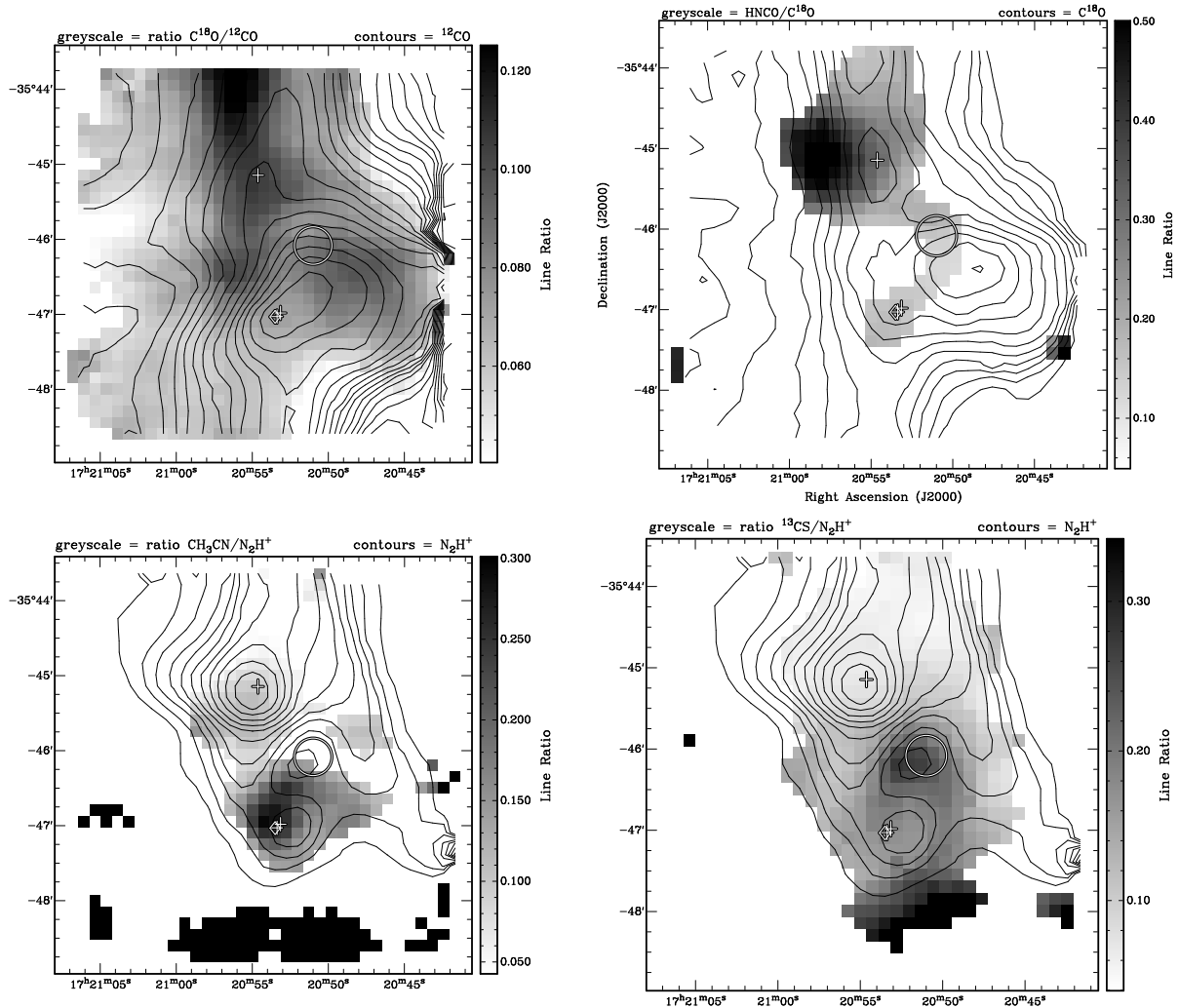


Figure 4. Line ratio maps. Upper-left shows the $\text{C}^{18}\text{O} (1-0)/^{12}\text{CO} (1-0)$ ratio in greyscale and $^{12}\text{CO} (1-0)$ integrated intensity in contours. Upper-right shows the $\text{HNCO} (5_{0,5}-4_{0,4})/\text{C}^{18}\text{O} (1-0)$ ratio in greyscale and $\text{C}^{18}\text{O} (1-0)$ integrated intensity in contours. Lower-left shows the $\text{CH}_3\text{CN} (5-4)/\text{N}_2\text{H}^+ (1-0)$ ratio in greyscale and $\text{N}_2\text{H}^+ (1-0)$ integrated intensity in contours. Lower-right shows the $^{13}\text{CS} (2-1)/\text{N}_2\text{H}^+ (1-0)$ ratio in greyscale and $\text{N}_2\text{H}^+ (1-0)$ integrated intensity in contours. Dark areas show high line ratios and light areas show low line ratios. The same contour levels as for Figure 3 have been used. Each ratio map is masked, based on the weaker image (the numerator), to reduce contributions due to non-real emission. However, non-real emission is seen at the bottom of the line ratio map for $\text{CH}_3\text{CN}/\text{N}_2\text{H}^+$ map, below the N_2H^+ contours.

gions in the map: a region to the east of NGC 6334 I(N) which shows a high ratio (ie. not a PDR) and a region including NGC 6334 I and E, which appears to be a good candidate PDR, although low signal in HNCO limits our interpretation beyond a narrow strip joining NGC 6334 I and E.

The lower-left image shows the $\text{CH}_3\text{CN}/\text{N}_2\text{H}^+$ line ratio map. As mentioned in §4.1, the CH_3CN emission is strongly confined to the centres of active star formation: NGC 6334 I and I(N), whereas N_2H^+ tends to trace ubiquitous and quiescent gas. The line ratio map clearly shows low line ratio towards NGC 6334 I, in contrast to a high ratio seen at NGC 6334 I(N). This demonstrates that I(N) is a more quiescent region, presumably with star formation at a younger stage.

The lower-right image shows the $^{13}\text{CS}/\text{N}_2\text{H}^+$ line ratio map. Here, we see the highest line ratio at the position of

the HII region NGC 6334 E. This is probably the result of N_2H^+ being destroyed by the HII region.

5 CONCLUSIONS

We have mapped a $5' \times 5'$ region, encompassing the high mass star formation sites NGC 6334 I and I(N). We have covered most of the 3 mm spectral window with these observations, using the Mopra radiotelescope. Our observations do not have sufficient spectral resolution to resolve spectral lines, but we compare morphologies of the various lines detected. We detect emission from 19 different molecules, ions and radicals, including multiple transitions of the same species and transitions from various isotopologues to yield a total of 52 spectral line detections.

We find that CH_3CN most closely follows the sites of

active star formation, although these sites feature prominently most other observed species. In contrast, emission from both CN and C₂H appear to be widespread and are good tracers of gas that is not associated with active star formation. N₂H⁺ and HC₃N morphologies closely resemble that of dust continuum emission, indicating that these two species are good tracers of column density, associated with both star forming sites and quiescent gas.

Interpretation of the emission from common species and their isotopologues (ie. CO, HCO⁺, HCN and HNC) are difficult to interpret, which is likely due to some transitions being optically thick. All CO isotopologues show a peak of emission about 45'' to the south-west of the HII region NGC 6334 E. However, this peak is not prominent in any other tracer, including dust continuum emission. We are currently unable to provide an explanation for this.

CH₃OH emission is seen in many transitions, including known Class I and II masers. Due to the low spatial resolution of these observations, we cannot conclude that we have detected any new masers amongst these new transitions. Thermal CH₃OH transitions show a marked difference in their occurrence: transitions with upper level kinetic temperatures above 100 K are found to be stronger towards NGC 6334 I and transitions with upper level kinetic temperatures below 22 K are found to be stronger towards NGC 6334 I(N). This supports the interpretation that NGC 6334 I is a more evolved site for star formation than I(N).

ACKNOWLEDGMENTS

The authors would like to thank Göran Sandell for providing the SCUBA continuum images shown in Figure 2. The Mopra Telescope is part of the Australia Telescope and is funded by the Commonwealth of Australia for operation as a National Facility managed by CSIRO. The University of New South Wales Mopra Spectrometer Digital Filter Bank used for the observations with the Mopra Telescope was provided with support from the Australian Research Council, together with the University of New South Wales, University of Sydney, Monash University and the CSIRO. H.B. acknowledges financial support by the Emmy-Noether-Program of the Deutsche Forschungsgemeinschaft (DFG, grant BE2578). The authors would like to thank the anonymous referee whose comments and suggestions have greatly improved the quality of this paper.

REFERENCES

- Bachiller, R. & Cernicharo, J. 1990, *ApJ*, 239, 276
 Beuther, H., Thorwirth, S., Zhang, Q., Hunter, T. R., Megeath, S. T., Walsh, A. J. & Menten, K. M. 2005, *ApJ*, 627, 834
 Beuther, H., Walsh, A. J., Thorwirth, S., Zhang, Q., Hunter, T. R., Megeath, S. T. & Menten, K. M. 2007, *A&A*, 466, 989
 Beuther, H., Semenov, D., Henning, Th. & Linz, H. 2008 *ApJL*, 675, 33
 Carral, P., Kurtz, S. E., Rodríguez, L. F., Menten, K., Cantó, J. & Arceo, R. 2002, *AJ*, 123, 2574
 Cheung, L., Frogel, J. A., Hauser, M. G. & Gezari, D. Y. 1978, *ApJL*, 226, 149
 Cragg, D. M., Sobolev, A. M., Ellingsen, S. P., Caswell, J. L., Godfrey, P. D., Saliu, S. V. & Dodson, R. G. 2001, *MNRAS*, 323, 939
 Garrod, R. T. & Herbst, E. 2006, *A&A*, 457, 927
 Gezari, D. Y. 1982, *ApJL*, 259, 29
 Herbst, E. & Leung, C. M. 1986, *MNRAS*, 222, 689
 Hunter, T. R., Brogan, C. L., Megeath, S. T., Menten, K. M., Beuther, H. & Thorwirth, S. 2006, *ApJ*, 649, 888
 Kraemer, K. E. & Jackson, J. M. 1999, *ApJS*, 124, 439
 Ladd, N., Purcell, C., Wong, T. & Robertson, S. 2005, *PASA*, 22, 62
 Leurini, S., Schilke, P., Parise, B., Wyrowski, F., Güsten, R. & Philipp, S. 2006, *A&AL*, 454, 83
 Lo, N., Cunningham, M., Bains, I., Burton, M. G. & Garay, G. 2007, *MNRAS Lett.*, 381, 30
 Martín, S., Requena-Torres, M. A., Martín-Pintado, J. & Mauersberger, R. 2008, *ApJ*, 678, 245
 McBreen, B., Fazio, G. G., Stier, M. & Wright, E. L. 1979, *ApJL*, 232, 183
 McCutcheon, W. H., Sandell, G., Matthews, H. E., Kuiper, T. B. H., Sutton, E. C., Danchi, W. C. & Sato, T. 2000, *MNRAS*, 316, 152
 Megeath, S. T. & Tieftrunk, A. R. 1999, *ApJL*, 526, 113
 Millar, T. J. & Nejad, L. A. M. 1985, *MNRAS*, 217, 507
 Müller, H. S. P., Thorwirth, S., Roth, D. A. & Winnewisser, G. 2001, *A&AL*, 370, 49
 Müller, H. S. P., Menten, K. M. & Mäder, H. 2004, *A&A*, 428, 1019
 Müller, H. S. P., Schlöder, F., Stutzki, J. & Winnewisser, G. 2005 *J. Mol. Struct.*, 742, 215
 Neckel, T. 1978, *A&A*, 69, 51
 Pickett, H. M., Poynter, R. L., Cohen, E. A., Delitsky, M. L., Pearson, J. C. & Müller, H. S. P. 1998 *J. Quant. Spectrosc. & Rad. Transfer*, 60, 883
 Rodríguez, L. F., Canto, J. & Moran, J. M. 1982, *ApJ*, 255, 103
 Rodríguez, L. F., Zapata, L. A. & Ho, P. T. P. 2007, *ApJL*, 654, 143
 Sandell, G. 2000, *A&A*, 358, 242
 Schilke, P., Comito, C., Thorwirth, S., Wyrowski, F., Menten, K. M., Güsten, R., Bergman, P. & Nyman, L.-Å. 2006, *A&AL*, 454, 41
 Sollins, P. K. & Megeath, S. T. 2004, *AJ*, 128, 2374
 Thorwirth, S., Winnewisser, G., Megeath, S. T. & Tieftrunk, A. R. 2003, *ASP Conf*, 287, 257
 Turner, B. E., Terzieva, R. & Herbst, E. 1999, *ApJ*, 518, 699
 Val'tts, I. E., Ellingsen, S. P., Slysh, V. I., Kalenskii, S. V., Otrupcek, R. & Voronkov, M. A. 1999, *MNRAS*, 310, 1077
 Val'tts, I. E., Ellingsen, S. P., Slysh, V. I., Kalenskii, S. V., Otrupcek, R. & Larionov, G. M. 2000, *MNRAS*, 317, 315
 Walsh, A. J., Burton, M. G., Hyland, A. R., Robinson, G., 1998, *MNRAS*, 301, 640
 Walsh, A. J., Burton, M. G., Hyland, A. R. & Robinson, G. 1999, *MNRAS*, 309, 905
 Zinchenko, I., Caselli, P. & Pirogov, L. 2009, *MNRAS*, 395, 2234

This paper has been typeset from a \TeX / \LaTeX file prepared by the author.